Journal of Molecular Catalysis A: Chemical 293 (2008) 31–38

Contents lists available at ScienceDirect

Journal of Molecular Catalysis A: Chemical

journal homepage: www.elsevier.com/locate/molcata

# Comparative study of transformation of linear alkanes over modified mordenites and sulphated zirconia catalysts: Influence of the zeolite acidity on the performance of *n*-butane isomerization

Alcineia C. Oliveira[a,*], Nadine Essayem[b], Alain Tuel[b], Jean-Marc Clacens[b], Younes Ben Tâarit[b]

[a] *Universidade Federal do Ceará, Campus do Pici-Bloco 940, Lab. Langmur de Adsorção e Catálise, 40.000.000 Fortaleza, Ceará, Brazil*
[b] *Institut de Recherches sur la Catalyse et l'Environnement de Lyon, IRCELyon Université Claude Bernard, Lyon1, 2 Av. Albert Einstein, 69626, Villeurbanne, France*

ARTICLE INFO

*Article history:*
Received 15 December 2007
Received in revised form 11 June 2008
Accepted 20 June 2008
Available online 27 June 2008

*Keywords:*
Dealuminated mordenite
Sulphate
Iron
NMR
*n*-Butane isomerization

ABSTRACT

Zeolite mordenite was dealuminated by steam treatment followed by acid leaching and further impregnated with 1 wt.% of iron or sulphated. The various solids were characterized by XRD, $^{29}$Si and $^{27}$Al NMR, IR of adsorbed pyridine as well as ammonia adsorption calorimetry and evaluated in *n*-butane isomerization. BET surface area of non-dealuminated mordenite was 462 $m^2\,g^{-1}$ and this value showed marked decreases if compared with the dealuminated (310 $m^2\,g^{-1}$), iron impregnated (302 $m^2\,g^{-1}$) and sulphated mordenite (247 $m^2\,g^{-1}$). It suggested the pore plugging or blocking by EFAL species, further confirmed by NMR experiments. The dealuminated mordenite showed Brønsted and Lewis acid sites with medium strength. The sulphated modified mordenite showed highest acidity strength, however its isomerization activity remains modest. The activity in the transformation of *n*-butane to isobutane was markedly improved by dealumination and subsequently iron impregnation (from $4 \times 10^{-9}$ to $2 \times 10^{-7}$ mol $s^{-1}\,g^{-1}$); a significant initial activity was observed at a temperature as low as 200 °C. At higher temperatures, the conversion level did not change. The positive effect of iron impregnation could be related to the increase in acid strength and/or to the participation of the redox properties of iron to the initial activation step of the reaction. Nevertheless, sulphated zirconia, used as a reference catalyst, presented the highest performance ($7 \times 10^{-7}$ mol $s^{-1}\,g^{-1}$) in comparison with modified mordenites.



## 1. Introduction

The isomerization of light paraffins is an important process for producing high-octane blending components in gasoline, with environmental regulations. As a typical acid-catalyzed reaction, the chlorinated alumina, heteropolyacid-based materials, sulphated zirconia and tungsten oxide on zirconia containing platinum have been shown to be active for carrying out the transformation of light alkanes [1]. However, owing to their acid properties and their shape selectivity and stability, zeolites promoted with Pt are the catalysts extensively used for the skeletal isomerization of light alkanes. Thus, over H-mordenite-based catalysts, the promotion with platinum improves considerably the activity, selectivity and stability with time on stream in the isomerization of light alkanes ($C_4$–$C_6$) [1,2]. Indeed, it is well known that light alkanes isomerization over non-modified Mordenite requires relatively high temperature to proceed via a monofunctional acid mechanism. Over Pt/zeolite, light alkanes isomerization occur more rapidly at moderate temperature, via a bifunctionnal metal-acid mechanism. The dehydrogenation abilities of the metallic sites generates olefins which are readily protonated over the Brønsted acid centers and converted into carbenium ions. Then , the isomerization process may proceed via classical acid catalyzed elementary steps.

A similar improvement in isomerization activity might be expected, if new active sites are generated nearby the zeolites Brønsted sites. These new sites should be able to generate a pool of carbocationic species by a pathway which would be energetically less demanding.

To reach that objective, it appeared interesting to evaluate two other directions. First, we assume that the presence of sites of highest strength might promote the zeolite isomerization activity, since the generation of the first carbocationic species might be favored. For that, we tentatively promoted Mordenite with sulphate groups. Second, since it is well known that the presence of re-dox sites could generate cationic radicals and then the required initial carbocationic species, we tentatively modified mordenite with iron.

* Corresponding author. Tel.: +55 85 33 66 90 41; fax: +55 85 33 66 99 82.
*E-mail address:* alcineia@ufc.br (A.C. Oliveira).

1381-1169/$ – see front matter © 2008 Elsevier B.V. All rights reserved.
doi:10.1016/j.molcata.2008.06.012

Mordenite was chosen according to its knwon efficiency in light alkane isomerization; this molecular sieve is a large pore 12-membered ring (MR) zeolite with a one-dimensional pore system [3–6]. The channel geometry consists of two types of pores parallel to one another one with a diameter of 2.6 Å × 5.7 Å and the other one with a diameter of 6.5 Å × 7.0 Å [3]. These two channels do not intersect, but small channels are accessible from the large ones by 8-rings windows. Also, mordenite has a total pore volume of approximately 0.2 mL $g^{-1}$. The specific pore geometry and the medium acidity make this zeolite potentially interesting for a variety of hydrocarbon conversion reactions such as isomerization [6], alkylation of aromatics [7], disproportionation [8] and transalkylation [9]. Among them, isomerization of *n*-butane to isobutane is a reaction that is generally carried out over strong Brønsted acidic materials like H-mordenite, sulphated zirconia or heteropycompounds [10]. The reaction of *n*-butane isomerization is represented by:

$$n\text{-}C_4H_{10} \rightleftarrows i\text{-}C_4H_{10} \quad \text{(I)}$$

It is generally accepted that the reaction occurs via a bimolecular mechanism over mordenite, involving a $C_8^+$ carbenium ion as intermediate [10,11]. Intramolecular rearrangement of *n*-$C_4$ alkane would require the formation of an unstable primary carbenium ion, which requires superacid sites. However, different routes have also been proposed, depending upon the reaction temperature and the concentration of the acid sites [6,12].

Generally, the main problem associated with the use of strongly acidic zeolites as isomerization catalysts is the fast rate of deactivation. Using hydrogen or water as additives into the feed stream combined with the modification of the zeolite with noble metals can partially circumvent this problem. The additives are used to prevent the formation of polymeric hydrocarbons or to help their decomposition and desorption.

In order to improve their isomerization activity, strong solid acids such as sulphated zirconia were successfully modified with low amounts of transition metals like Fe and/or Mn. These metals were proposed to promote a bifunctional mechanism, where the redox properties of the transition element could initiate the alkane conversion [13]. Although enormous work has been reported on the isomerization properties of mordenite zeolite, very little information has been reported in open literature on the modification of this zeolite with sulphated groups or transition metals such as Fe and Mn in the *n*-butane transformation [2,12–14], in order to enhance its catalytic activity.

The present study focuses on the use of modified mordenite for the *n*-butane isomerization. Mordenite was first dealuminated and then impregnated with iron or sulphate. Dealumination is a well-known method for enhancing the acidity and accessibility of active sites in zeolites [15]. Iron compounds are extensively used as catalysts in industrial processes due to their chemical properties and low cost. Both the dealumination and iron incorporation were expected to enhance the mordenite performance in the *n*-butane isomerization. It was also shown that sulphated mordenites are active for catalytic reactions involving bulky organic compounds, showing different activities and selectivities, depending on their acidity and active sites accessibility [16]. Therefore, the structural changes resulting from the mordenite modifications as well as the acid properties of the catalysts were studied and correlated with the *n*-$C_4$ isomerization activity.

## 2. Experimental

### 2.1. Samples preparation

Na-mordenite was obtained from Societé Chimique Grande Paroisse with a Si/Al ratio of 6.3, a BET surface area of 450 $m^{-2}$ $g^{-1}$ and a sodium content of 3.2 wt.%. The sodium modernite was converted into the acidic form by treatment with a 0.5 mol $L^{-1}$ HCl solution at 80 °C for 1 h. The solid was then dried at 80 °C and calcined at 500 °C under nitrogen/air flow. The protonic mordenite sample was labelled M. Dealumination was performed on the exchanged solid as proposed by Almanza et al. [6] by using a steam partial pressure of 12.5 kPa, for approximately 9 h. The solid was then refluxed in hydrochloric acid (3 mol $L^{-1}$) at 80 °C for 1 h and subsequently washed in order to remove chloride species. A final calcination was performed under air at 500 °C for 2 h, leading to the dealuminated mordenite sample, labelled M1.

An iron impregnated mordenite was prepared from M1 by using a 0.1 mol $L^{-1}$ iron nitrate solution to obtain a concentration of Fe of 1 wt.%. Iron impregnation was carried out under stirring for 1 h, followed by vacuum filtration and drying at 80 °C. The solid was then calcined under air flow at 500 °C for 2 h, leading to sample FeM1 (iron impregnated dealuminated modernite).

A sulphated mordenite ($SO_4$M1) was prepared by treating 1 g of M1 with a 0.1 mol $L^{-1}$ sulphuric acid solution (50 mL of solution for 1 g of M1). The impregnation of M1 with the sulphate was carried out under stirring during 4 h, with a buffer (pH 3–5) followed by vacuum filtration and drying at 80 °C. The solid was then calcined under air flow at 500 °C for 2 h. Following each step, the crystallinity of the solids was evaluated by X-ray diffraction.

A sulphated zirconia ($SO_4$Z) was synthesized according to the literature [17], by using zirconium hydroxide with a 0.2N sulphuric acid solution. This solid was used as control catalyst. Its specific surface area (BET) is equal to 100 $m^2$ $g^{-1}$. The protonic density drawn from $NH_3$ adsorption at 373 K is equal to 22 × $10^{17}$ $H^+$ $m^{-2}$ [1].

### 2.2. Characterization

All solids were characterized by XRD, chemical analysis, nitrogen adsorption at 77 K, microcalorimetry adsorption of ammonia, pyridine adsorption, NMR and *n*-butane isomerization as a test reaction.

The chemical analyses were performed on a Carry AAS/ICP OES instrument. Each sample was dissolved in HF:HCl solutions, before measurement of the chemical composition.

X-ray diffraction (XRD) patterns were colleted on a Bruker (Siemens) D5005 diffractometer by using the Cu Kα radiation, at a work voltage of 40 kV and current was 40 mA.

BET measurements were recorded on a Micromeretics ASAP 2002 equipment. Samples were first treated in vacuum to remove the gaseous impurities (300 °C, 6 h, $10^{-3}$ Torr) and the textural features were studied by using nitrogen adsorption at 77 K.

NMR experiments were carried out on a Bruker DSX 400 spectrometer. Samples were spun at 10 kHz in 4 nm zirconia rotors. $^{27}Al$ and $^{29}Si$ chemical shifts were referenced to $Al(H_2O)_6^{3+}$ and tetramethylsilane (TMS), respectively.

### 2.3. Acidity measurements

Pyridine adsorption–desorption was monitored by infrared spectroscopy (IR). Self-supported wafers of 20 mg and 18 mm diameter were evacuated *in situ* in an infrared glass vacuum cell equipped with calcium fluoride windows. The cell was then connected to a vacuum system and the samples were degassed under $10^{-5}$ Torr at 450 °C for 4 h. IR spectra were recorded before as well as after pyridine adsorption at room temperature. Pyridine was then desorbed at increasing temperatures (150, 250, 350, and 450 °C) in dynamic vacuum and spectra were recorded on a Bruker Vector 22 (IRFT) spectrometer.

Calorimetry of ammonia adsorption was performed in a tubular cell preliminary heated at 400 °C under vacuum for 2 h. The cell

was then introduced in a Setaram Soft Set 2000 calorimeter at 80 °C and the experiment was performed. Successive ammonia injections were done until complete saturation of the sample.

The isomerization of *n*-butane was used as a test reaction. The samples 100 mg in weight were placed in a tubular quartz reactor and heated at 400 °C under air flow (0.3 L $h^{-1}$) for 2 h. The reaction was carried out at 200 or 250 °C, by using a butane/nitrogen mixture (5% *n*-$C_4$ in $N_2$, total flow rate of 1.28 L $h^{-1}$) and the products were analyzed by a DELSI chromatograph with a flame ionisation detector coupled to a Merck D2500 integrator.

## 3. Results and discussion

### 3.1. XRD analysis

XRD patterns of the various mordenites show that the structure is maintained in all samples. The ion exchange from Na to H form and the subsequent calcination of M sample do not affect the crystallinity (Fig. 1).

In particular, dealumination by steaming, followed by acid leaching to obtain M1 does not affect the crystallinity of the zeolite. Moreover, neither iron impregnation (FeM1) nor sulphatation ($SO_4$M1) of the M1 sample causes any significant loss of crystallinity.

### 3.2. Physico-chemical properties of the solids

The non-dealuminated protonic mordenite (M) possesses a type I isotherm, characteristic of a microporous material, as reported in a previous work [16]. The modification of the protonic mordenite by combination of hydrothermal treatment and acid leaching (M1) resulted in a dramatic difference in the isotherm shape, which passed from type I to type IV, indicating the presence of mesopores formed upon dealumination. The above conclusions are in line with previous findings [15]. The textural features of the solids evaluated from $N_2$ isotherms are given in Table 1.

The M sample has a surface area of 462 $m^2\,g^{-1}$ and micropore volume of 0.23 mL $g^{-1}$ and these values show marked decrease if compared with the dealuminated (310 $m^2\,g^{-1}$, 0.13 mL $g^{-1}$) iron impregnated (302 $m^2\,g^{-1}$, 0.12 mL $g^{-1}$) and sulphated modernite (247 $m^2\,g^{-1}$, 0.10 mL $g^{-1}$). It suggests the pore plugging or blocking by EFAL species, further confirmed by NMR results. Mesopores are not found on the M sample. By contrast, modified mordenites present mesopores and FeM1 shows a decrease in both the micro- and meso-pore volumes, as compared to M1. The presence of iron (1 wt.%) does not significantly modify the textural parameters. The absence of any diffraction peak related to Fe particles suggests that iron is occluded as fine oxides inside the modernite mesopores as finely dispersed octahedral $Fe^{3+}$ species. Thus, it explains the slight decrease in the textural parameters for the FeM1 sample. Indeed, the textural features of the $SO_4$M1 sample are a result from the presence of sulphate ions, which may partially block the access to some of the mesopores.

The Si/Al ratio slight increases from M1 to FeM1, suggesting that iron impregnation removes some aluminum species from the zeolite. For the $SO_4$M1 sample, a considerable increase in the Si/Al ratio is observed, suggesting that the sulphatation removes aluminium from the sample, probably in the form of soluble aluminium sulphate.

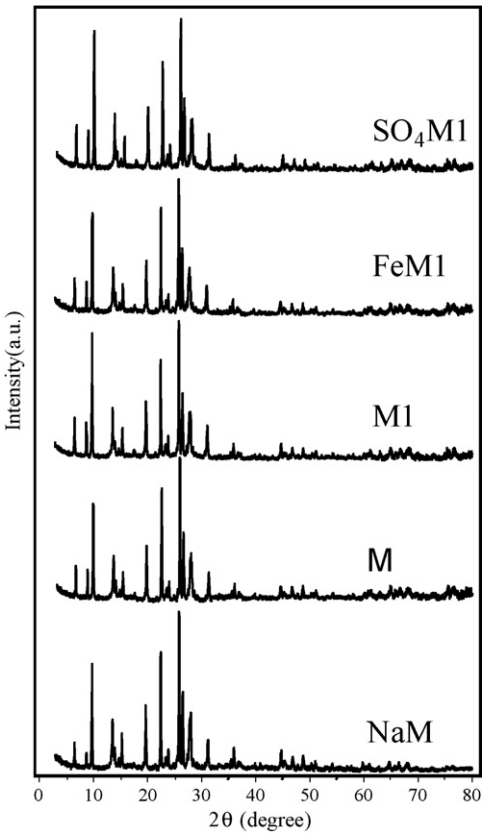


**Fig. 1.** XRD patterns of the modernites studied in this work. Samples: non-dealuminated modernite containg sodium (NaM), protonic non-dealuminated modernite (M), dealuminated modernite (M1), iron impregnated dealuminated mordenite (FeM1) and sulphated dealuminated mordenite ($SO_4$M1).

The $^{29}$Si NMR spectrum of M is composed of three signals corresponding to Si(0Al) at −112 ppm, Si(1Al) at −105 ppm and Si (2Al) at −100 ppm. For the modified mordenites samples, the band at −110 ppm is split into two components, characteristic of severely dealuminated mordenites [15,16].

The $^{27}$Al NMR spectra (Fig. 2) show a sharp resonance peak at 55 ppm for all samples, which is related to structural tetrahedral aluminium species. A weaker resonance is also observed at 0 ppm, characteristic of aluminium atoms in octahedral coordination or in extra framework position. Extraframework aluminium species (EFAL) remain even after acid leaching of the dealuminated sample (M1), suggesting that these species are difficult to remove and that they could be located in the 8-MR pores of the structure.

In addition to the peak at 0 ppm, M1 shows a new peak at 30 ppm assigned to pentacoordinated aluminium species, suggesting that the dealumination leads to a structural disorder in the solid. Iron impregnation or sulphatation decrease the amount of extraframe-

**Table 1**
Chemical composition and the textural properties of the solids

| Sample | Si/Al | Fe (wt.%) | *S* (wt.%) | $S_{BET}$ ($m^2\,g^{-1}$) | $V_{micro}$ (mL $g^{-1}$) | $V_{meso}$ (mL $g^{-1}$) |
|---|---|---|---|---|---|---|
| M | 6 | – | – | 462 | 0.23 | 0 |
| M1 | 13 | – | – | 310 | 0.13 | 0.054 |
| FeM1 | 15 | 0.95 | – | 302 | 0.12 | 0.046 |
| $SO_4$M1 | 20 | – | 1.2 | 247 | 0.10 | 0.043 |

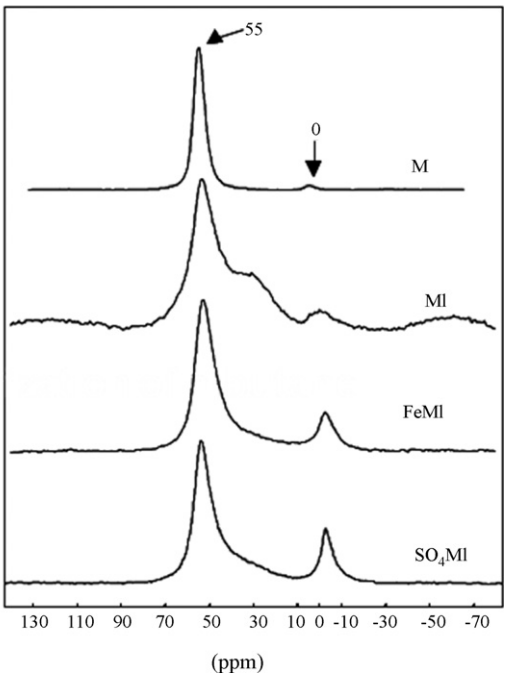


**Fig. 2.** $^{27}$Al NMR spectra of non-dealuminated mordenite (M), dealuminated mordenite (M1) iron impregnated dealuminated mordenite (FeM1) and sulphated dealuminated mordenite ($SO_4$M1).

work species, particularly the 5-coordinate species. From the above study, we can conclude that the successive modifications of a mordenite did not cause any loss of crystallinity, but generated structural defects in the materials, essentially a secondary mesopore system, as seen in the textural analysis results.

### 3.3. Acidity measurements

#### 3.3.1. Calorimetry

Calorimetry is a well-suited technique to probe the concentration and strength of acid sites on the surface of solid catalysts. Calorimetry results on the M sample shows a large number of acid sites, mainly with a medium strength. The dealumination process leads to an increase in the strength of the sites, but the latter remain in a relative homogeneous strength on the surface, as shown in the M1 sample (Fig. 3).

This suggests that dealumination provides an increase in the strength of the sites, but that the latter remain in a relative homogeneous strength on the surface and accessible to the ammonia molecule. We can also remark the difficulty for the first doses of ammonia to access the acid sites, probably due to steric hindrance caused by the EFAL species present on the solid. As the ammonia amount increases, the accessibility of the referred sonde molecule to the acid sites is improved and then the measurement is performed. FeM1 presents acid sites with medium and highest strengths, but with a population not as homogeneous as in the case of M1 (Fig. 4).

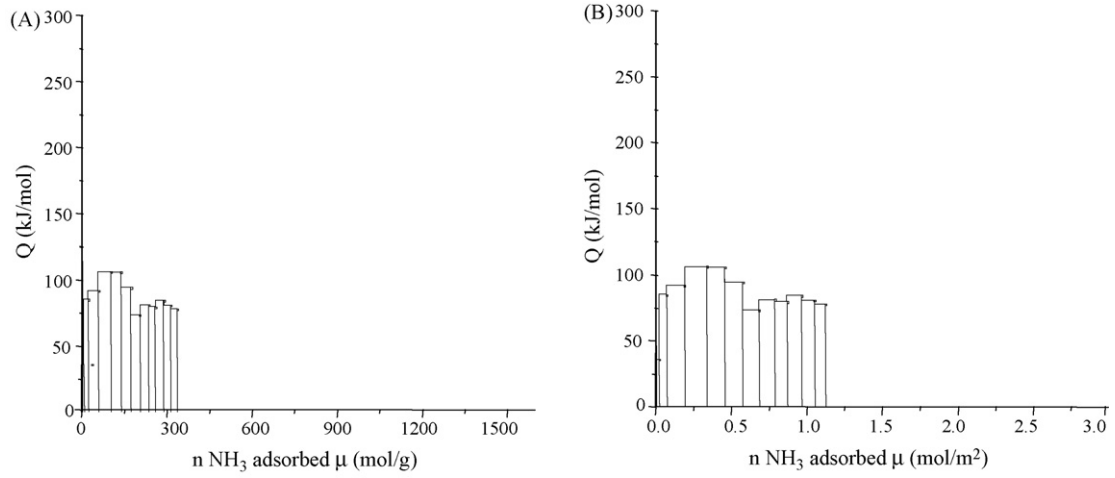


**Fig. 3.** Calorimetric diagram of the dealuminated mordenite sample (M1). Micromol of ammonia adsorbed per gram (A) and per square meter (B) of the catalyst.

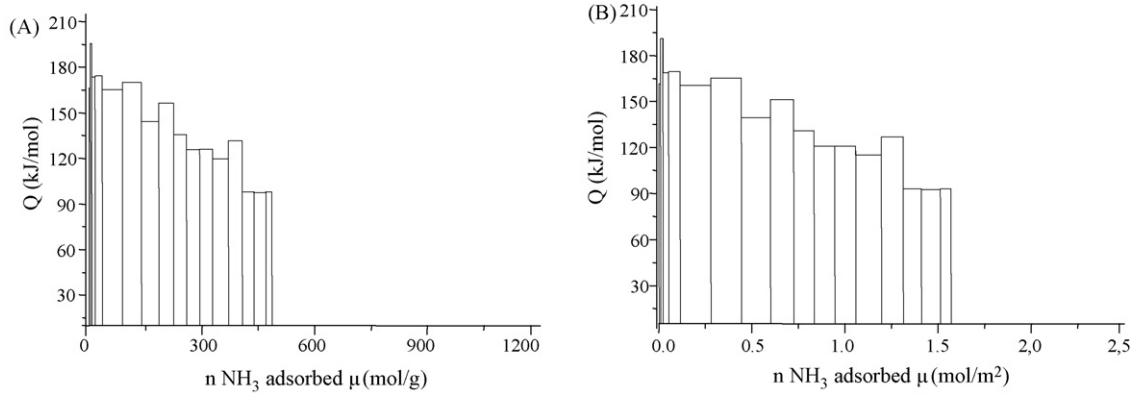


**Fig. 4.** Calorimetric diagram of the iron impregnated dealuminated mordenite (FeM1) sample. Micromol of ammonia adsorbed per gram (A) and per square meter (B) of the catalyst.

In the case of $SO_4$M1, calorimetry results also presents acid sites with high strength compared to M1 and FeM1, but with a population not as homogeneous as the latter. The accessibility of ammonia to the acid sites is restricted due to the interaction between ammonia and sulphate ions or EFAL species, as seen by NMR results and confirmed previously [16].

### 3.3.2. Py adsorption

Pyridine is a useful basic probe molecule to distinguish the nature (Brønsted and Lewis), the location and the number of accessible acid sites [17,18]. Fig. 5 shows the IR spectra of the various mordenites before Py adsorption.

The samples show the characteristic bands of a protonic zeolite: at 3744 $cm^{-1}$ (terminal SiOH groups) and at 3607 $cm^{-1}$ (acid bridging Si–O(H)–Al groups). Preliminary works showed that dealumination generally provides a decrease in the band at 3607 $cm^{-1}$, while the band at 3744 $cm^{-1}$ increases in intensity [18]. These results are partially in line with the spectra of the M1, FeM1 and $SO_4$M1 samples. It can be explained by the fact that removal of aluminum atoms from the zeolite framework decreases the number of bridging protons. However, we do not observe a parallel rise of the terminal silanol stretching vibration. Interestingly, the intensity of the band at 3744 $cm^{-1}$ is increased and it suggests a further dealumination of the $SO_4$M1 sample.

In addition, two news bands appear at 3710 $cm^{-1}$ and at 3650 $cm^{-1}$ in the spectra of the modified solids. The first band results from the formation of hydroxyl nests, formed upon dealumination of the zeolite. The second one is most likely due to hydroxyl groups of extraframework aluminum species such as $Al(OH)_4$, $Al(OH)^{2+}$ and $Al(OH)^{4+}$ species [18].

Upon addition of pyridine to the non-dealuminated mordenite (M), there is no absorption band near 1455 $cm^{-1}$, which indicates the absence of Lewis sites (Fig. 6). The band corresponding to Si–O–(H)–Al groups is not completely eliminated upon pyridine adsorption, which means that most of the acid sites are located in the small channels of the non-dealuminated mordenite. By contrast, in the case of modified samples (M1 and FeM1), the band at 3607 $cm^{-1}$ completely disappears. This indicates that most of the acid sites that are located in the small channels and that are not accessible to pyridine (size of the molecule 5.8 Å) become more exposed upon dealumination. Simultaneously, a band at 1545 $cm^{-1}$, characteristic of pyridinium ions, appears in the spectra of these samples, as seen in Fig. 6.

By contrast, for the $SO_4$M1 sample, the bridged silanols vibration at 3607 $cm^{-1}$ is not completely eliminated after addition of pyridine at room temperature. It suggests that some of the acid sites are blocked by EFAL species, as seen by NMR experiments that showed a large amount of these species. Another possibility is that the acid sites could be in the small channels, and not accessible to pyridine.

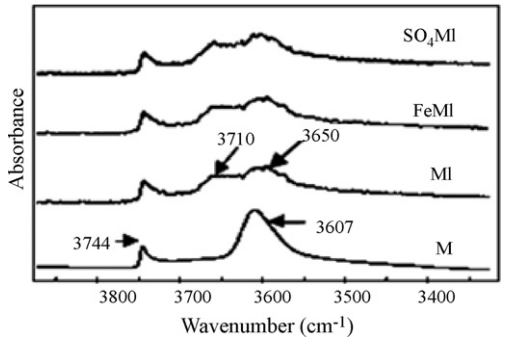


**Fig. 5.** IR spectra of the hydroxyl stretching vibrations region before pyridine adsorption. Samples were treated at 450 °C, under $10^{-3}$ Torr.

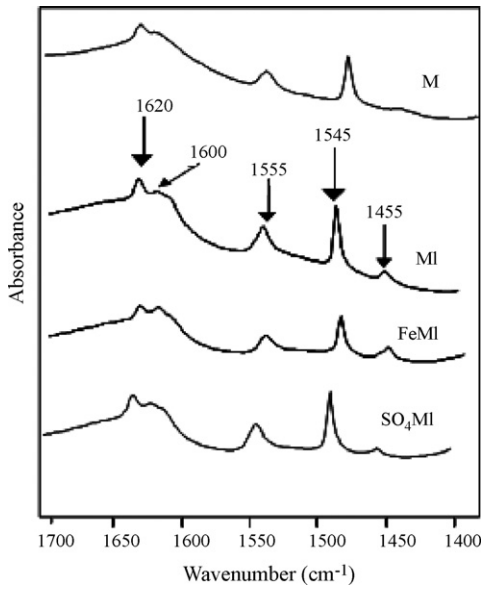


**Fig. 6.** IR spectra after pyridine adsorption. Samples were desorbed at 150 °C.

According to the spectra recorded after desorption at 150 °C (Fig. 6), the modified mordenites show the presence of a band at 1455 $cm^{-1}$ that indicates the presence of Lewis acid sites.

In addition, a band at 1620 $cm^{-1}$ is related to the presence of Lewis acid sites and another band at 1600 $cm^{-1}$ is assigned to other type of Lewis acid sites. Both bands related to Lewis acid sites are supposed to be associated with extraframework aluminum species. Increasing the temperature of desorption decreases the amount of Brønsted sites, and only Lewis sites remain at 450 °C. Either iron impregnation or sulphatation of the dealuminated mordenite does not modify significantly the nature of the acid sites, as evidenced by pyridine adsorption results.

On the other hand, the acid properties evidenced by calorimetry clearly show that iron impregnation increases the strength of the acid sites. Fe incorporation in the dealuminated mordenite is found to improve the overall acid strength without significant changes in the amount and nature of the sites. A possible explanation may be that the Lewis acidity of iron influences the overall acidity of the zeolite. Indeed, when properly positioned, Lewis centres can increase the strength of Brønsted acid sites, as described in zeolite literature [19].

Upon sulphatation, the Lewis/Brønsted ratio was not changed. However, the total acidity of the solid was enhanced. Therefore, the acidity strength studied by pyridine adsorption measurements follows the order: $SO_4$M1∼ FeM1 > M1 > M.

These results suggest that dealumination increases the accessibility to Brønsted sites of the zeolite, in agreement with calorimetry results. The sulphatation or iron addition does not modify the L/B ratio. Upon Fe promotion, the significant acid strength improvement revealed by calorimetry, is originated from the interaction between new Lewis acid centers, $Fe^{3+}$, with the silanol groups. This results in an increase of the strength of the Brønsted sites and it can be the origin of the improved overall acid strength revealed by calorimetry experiments.

## 3.4. Performance in the n-butane isomerization

### 3.4.1. Evaluation of the solids at low temperature

Isomerization of *n*-butane to isobutane was chosen as a model reaction to test the catalytic activity of the various zeolites. For this reaction, strong acid sites are generally required [20,21]. Prior to

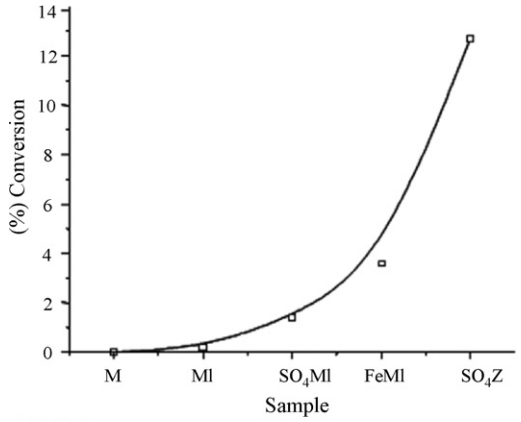


**Fig. 7.** Conversion of *n*-butane to various solids studied.

catalytic tests, the samples were embedded with a binder, and we ensured that the binder did not interfere in the catalyst activity. Catalytic results are shown in Fig. 7.

The M sample is not active in the reaction due to its low acidity and pore geometry restrictions. This result is in accordance with the effect of the pore geometry on isomerization mechanism of *n*-butane that has been intensively studied for one-dimensional H-modernite [22]. The findings reported that in such one-dimensional pore system, with acid sites of comparable strength of the M sample, the monomolecular reactions involving *n*-butane are *single file* diffusion controlled. In other words, the H-modernite has the main channel of 6.5 Å × 7.0 Å of diameter that is close to the kinetic diameters of *n*-butane and isobutane (4.3 and 5.0 Å, respectively). Thus, the reaction products can leave an acid site in the interior of the one-dimensional channel of protonic modernite, only if no other molecules block the space between the reaction site and pore mouth. The only reactions products that are detected are those generated at active sites near to the pore mouth, being the products formed inside the pore trapped [22,23]. It could explain the lack of activity of the M sample.

In spite of its high acidity, M1 shows a low performance, may be due to the fact that some of the acid sites are still present in the narrow pore of the zeolite, and may suffer from restrictive accessibility as regard to the possible $C_8^+$ intermediate formation, if the mechanism proceeds via a bimolecular acid step [2]. Although the M1 sample has a three-dimensional pore system as a result of dealumination, the large amount of EFAL species (observed by means of NMR measurements) may be located inside the pore. Therefore, the $C_8^+$ bulk intermediate from a bimolecular process will be very difficult inside the pore of dealuminated modernite. This way, the catalytic activity is no longer controlled by the density, but by the accessibility of the active sites, as seen in early studies [24]. Indeed, the strength of the acid site is probably too low and does not permit the *n*-butane isomerization by a monomolecular mechanism over the M1 sample; therefore, this support the hypothesis of the bimolecular mechanism at the condition studied.

The initial conversion level is intensified by sulphatation (1.2%) of the dealuminated sample. It can be ascribed to the balance between the strong acid sites, created upon sulphatation, and the mesopore system that permits the accessibility of the reactants to the acid sites. It is well known that in the case of sulphated oxides, superacidity from the presence of Brønsted sites, whose acidity is enhanced by the presence of strong neighboring Lewis acid sites [2,21]. Our results for $SO_4$M1 show a large amount of EFAL species produced by progressive dealumination which is caused by $SO_4$ ions. Taking all this into account, it could be expected that both sulphate ions and EFAL species improved the acid strength of Brønsted acid sites over $SO_4$M1. As consequence, the catalytic activity of this sample is enhanced, in comparison with the M and M1 samples.

From the analysis through calorimetry, it is also seen that $SO_4$M1 has strong acidity ($E_a$ $NH_3$ = 150–170 kJ mol$^{-1}$), as shown previously [16] and IR pyridine adsorption studies reveal the presence of strong Brønsted acid sites, which has a great accessibility, in comparison to non-dealuminated and dealuminated zeolites. Thus, the catalytic activity of $SO_4$M1 is believed to be generated by the presence of the strong Brønsted acid sites.

However, the conversion level is considered too low, by considering the acidity features of the $SO_4$M1 sample. The catalytic performance drastically deteriorates with the reaction time, in a similar manner to that occurs to the sulphated oxides [1].

In contrast, the FeM1 sample shows an initial *n*-butane conversion of 3.6%. The findings reports that when iron is introduced in mordenites followed by a calcination under air condition, $Fe^{3+}$ ions can be located in charge compensating positions or became non lattice species, being octahedral iron oxides [25–30]. Another possibility is that iron is incorporated in the framework of modernite [27,29], but because $Fe^{3+}$ has a larger ionic radius (0.63 Å) than $Al^{3+}$ (0.53 Å), this possibility is unlikely. XRD results suggest that the octahedral $Fe^{3+}$ species are not only in the form of highly dispersed particles but also are deep inside the channels, as evidenced by the textural parameters that show the pore plugging or blocking, probably caused by iron species on the FeM1 sample. The oxidized species may not be attached strongly to the modernite and can generate an additional acidity as Lewis acidic center, thus providing the catalytic activity of the FeM1 sample.

The difference in the acidic features, mainly in terms of acid strength of FeM1 compared to $SO_4$M1, could explain the better performance of the iron impregnated mordenite since the *n*-$C_4$ transformation is catalyzed by strong acid sites. However, we cannot exclude the participation of a redox initial activation step due to non-framework $Fe^{3+}$ species in the iron modified mordenite, as seen earlier [2,13]. A greater stabilization of the highest transition state on FeM1 than on $SO_4$M1 is a possibility, but isomerization over the FeM1 catalyst apparently can occur by oligomerization and β-fission of a chemisorbed $C_8$-carbenium ion to *iso*-$C_4$ fragments, according to the studies focused on Fe species on zirconia catalysts [30].

Nevertheless, the highest conversion is observed with the reference sulphated zirconia catalyst that possesses a strong acidity. The initial conversion level obtained with the $SO_4$Z sample reaches 12.7% under similar experimental conditions (Fig. 7). The structure of the active site in *n*-butane isomerization is still under controversy [21], but under similar condition studied, a bimolecular mechanism on pentacoordinated sites could work.

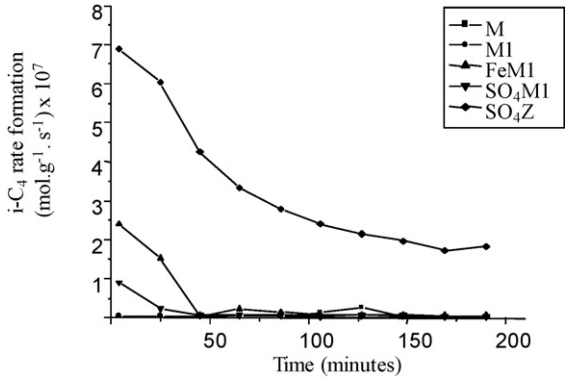


**Fig. 8.** Rate of isobutane formation with time on stream. Conditions: treatment: 2 h under air at 200 °C. Total flow rate = 1.3 L h$^{-1}$; m catalyst = 100 mg. Five percent of *n*-$C_4$ in $N_2$; TR = 200 °C.

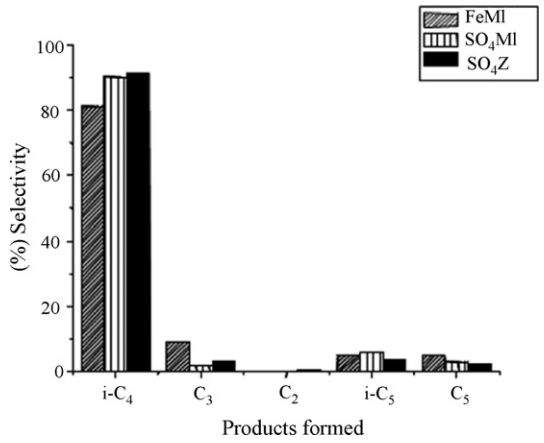


**Fig. 9.** Selectivities of the various catalysts in the *n*-butane isomerization. *i*-$C_4$, $C_3$, $C_2$, *i*-$C_5$ and $C_5$ represent the selectivities to isobutane, propane, ethane, isopentane and pentane, respectively.

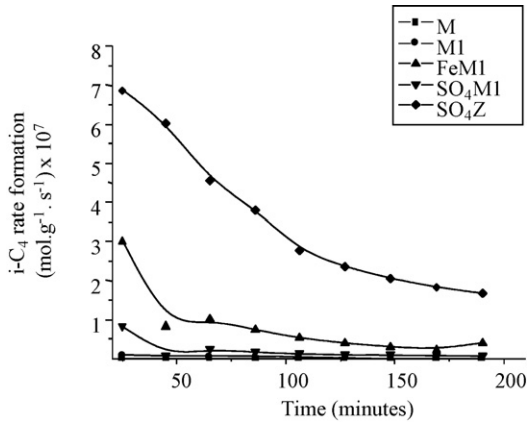


**Fig. 10.** Rate of isobutane formation with time on stream. Conditions: treatment: 2 h under air at 200 °C. Total flow rate = 1.3 L $h^{-1}$; *m* catalyst = 100 mg. 5% *n*-$C_4$ in $N_2$; TR = 250 °C.

Additionally, previous experiments have demonstrated that a (gamma) alumina, a sulphated (gamma) alumina samples are inactive to isomerize *n*-butane, probably because they are only mildly acidic, with regard the strength required to initiate the isomerization. The rate of isobutane formation, expressed as the moles of *n*-butane formed per second and per gram catalyst, has been plotted as a function of the reaction time (Fig. 8).

The rate of formation of isobutane, which reflects the performance of the catalysts, is only three times as high on the sulfated zirconia ($6.8 \times 10^{-7}$ mol $s^{-1}$ $g^{-1}$) as on the FeM1 sample. Although the reference $SO_4Z$ catalyst shows the best performance due to its strong acid sites, it also rapidly deactivates. This can be related to the poisoning of the acid sites by coke precursors, as suggested by the dark grey color of the used sample.

The selectivities obtained with M and M1 are meaningless because the conversion level is too low. On the other hand, the major product obtained with FeM1, $SO_4$M1 and $SO_4Z$ samples is isobutane (Fig. 9), indicating a deprotonation equilibria (reaction II) can occur.

By-products being mainly propane, isopentane and pentane are also formed. Light alkanes such as ethane are hardly formed. The presence of these by-products strongly supports the bimolecular dimerization-cracking pathway, where the $C_8^+$ carbenium intermediate is formed (reaction III) and then cracked into lighter fragments, principally $C_5$ and $C_3$ (reaction IV).

$$C_4H_{10} \rightleftharpoons C_4H_9^+ + H^+ \quad \text{(II)}$$

$$2C_4H_9^+ \rightarrow C_8H_{17}^+ + H^+ \quad \text{(III)}$$

$$C_8H_{17}^+ + H^+ \rightarrow C_3H_8 + C_5H_{10} \quad \text{(IV)}$$

*3.4.2. Evaluation of the solids at 250 °C*

The rate of isobutane formation at higher temperatures, with time is shown in Fig. 10.

The isobutane production slightly increases with the increase in temperature. The stabilities of the catalysts evaluated are not improved by the iron impregnation or sulphatation. In principle, with such a variety of solids one can except to see some trends between the zeolite acidity and their behaviour as potential catalysts in *n*-butane transformation. Thus, the acid sites present in the dealuminated mordenite (M1 sample) are expected to influence the isobutane formation and the product distribution all along the reaction time, but only the iron-modified zeolite shows a significant activity at 250 °C.

The new sites generated by iron impregnation are not able to maintain the activity of the catalyst which rapidly decreases with time. The activity of FeM1 can be ascribed to its high acid strength as compared to M1 and/or to the participation of the iron redox properties in the initial *n*-$C_4$ activation step. However, a redox initial activation step would have generated a butyl radical cation as intermediate that reacts with a butane molecule by forming a $C_8^+$ intermediate and a proton. Thus, it is worth pointing out that over zeolites, isobutane can be formed though a cracking mechanism which can be carried out on Brønsted acid sites and that together with cracking, addition (reaction V) and specially, oligomerization reactions also occur.

$$C_4H_9^+ + C_4H_{10} \rightarrow C_8H_{18} + H^+ \quad \text{(V)}$$

This hypothesis is supported by the large amount of *i*-$C_4$ found over the FeM1 sample at 250 °C, but iron and EFAL Lewis sites plus strong Brønsted acid sites present on this sample are not able to maintain the isobutane production along of the time, probably due to the carbon deposition.

Because acid catalyzed reactions of cracking are favourable at high temperature, the amount of side products such as ethane and propane is increased and it suggest that a monomolecular mechanism could take place over the Brønsted acid sites of $SO_4Z$, e.g., via pentacoordinated carbenium ion as proposed [2,31]:

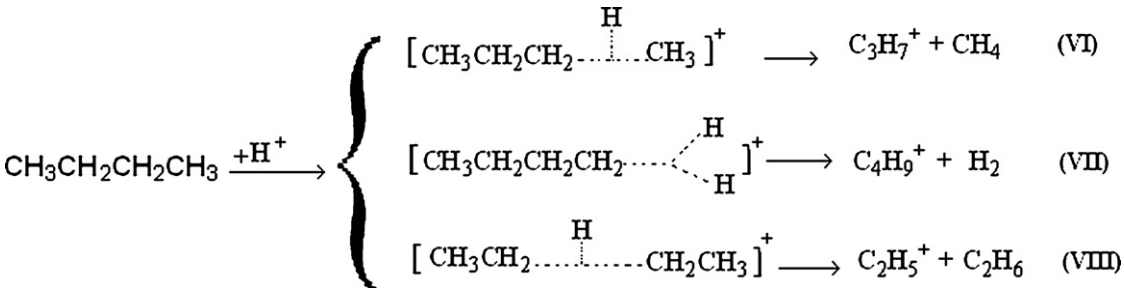

In summary, it can be observed that sulphated zirconia is able to isomerize *n*-butane to isobutane owing to its higher acidity and stability as compared with dealuminated mordenites. In contrast, sulphated zirconia cannot act as an adequate isomerization catalyst for *n*-butane. transformation since it is poisoned by coke and thus reduces the formation of isobutane.

## 4. Conclusions

The modification of a mordenite by dealumination creates some mesoporosity, which considerably improves the accessibility to active site as compared to a standard zeolite. The subsequent impregnation of the catalyst with iron alters neither the mesopore system nor the zeolite crystallinity. However, iron impregnation or sulphatation increases the acid strength of the zeolite. Neither the non-dealuminated nor non-doped dealuminated mordenite is able to catalyze the *n*-butane isomerization at a reaction temperature as low as 200 °C. Despite its strong Brønsted acid sites, the sulphated zeolite shows a modest activity. On the other hand, the iron-impregnated zeolite possesses acid sites capable of catalyzing the *n*-butane transformation.

The improvement of the acid strength evidenced by calorimetry is tentatively explained by a synergistic effect between the iron Lewis sites and the Brønsted acid sites of the modified zeolite. However, based on the present data only, we cannot conclude whether the improvement of the catalytic performance of iron impregnation on dealuminated mordenite is related to the increase in the acid strength through iron incorporation and/or to the participation of redox $n$-$C_4$ initial activation step. Nevertheless,a classical sulphated zirconia evaluated as a reference catalyst exhibited the best stability and catalytic performance towards isobutane production among the solids studied.

The characteristics of the modified mordenites in terms of acidity, redox properties and accessibility possibly make these solids useful for catalytic reactions involving bulky organic compounds.

## Acknowledgments

The authors wish to acknowledge CAPES/CNPq for A.C.O phd scholarship as well as CNRS by funding of this research.

## References

[1] N. Essayem, Y. Ben Taârit, C. Feche, P.Y. Gayraud, G. Sapaly, C. Naccache, J. Catal. 219 (2003) 97–106.
[2] A. Corma, Chem. Rev. 95 (1995) 559–614.
[3] C. Baerlocher, W.M. Meier, D.H. Olson, Atlas of Zeolite Structure Types, Atlas of Zeolite Framework Types, 6th ed., Elsevier, Amsterdam, 2007, pp. 218–219.
[4] N.C. Satterfield, Heterogenous Catalysis in Pratice, Mc Graw Hill Book Company, New York, 1978, p. 168.
[5] L. Smart, E. Moore, Solid State Chemistry, An Introduction, Chapman & Hall, 1992, p. 203.
[6] L.O. Almanza, T. Narbeshuber, P. d'Araujo, C. Naccache, Y. Ben Taârit, Appl. Catal. A: Gen. 178 (1999) 39–47.
[7] R. Anand, R. Maheswari, S.G. Hegde, B.S. Rao, J. Mol. Catal. A: Chem. 192 (2003) 253–262.
[8] Y.-K. Lee, S.-H. Park, H.-K. Rhee, Catal. Today 44 (1998) 223–233.
[9] T.C. Tsai, B.S. Liu, I. Wang, Appl. Catal. A: Gen. 181 (1999) 355–398.
[10] M. Guisnet, Ph. Bichon, N.S. Gnep, N. Essayem, Top. Catal. 11 (2000) 247–254.
[11] J.C. Yori, M.A. D'Amato, G. Costa, J.M. Parera, React. Kinet. Catal. Lett. 56 (1995) 129–135.
[12] R.A. Asguo, G. E-Mirth, K. Seshan, J.A. Pieterse, J.A. Lercher, J. Catal. 168 (1997) 292–300.
[13] K.T. Wam, C.B. Khouw, M.E. Davis, J. Catal. 158 (1996) 311–326.
[14] C.-L. Chen, S. Cheng, H.-P. Lin, S.-T. Wong, C.-Y. Mou, Appl. Catal. A: Gen. 215 (2001) 21–30.
[15] I. Ivanova, V. Montouillout, C. Fernandez, O. Marie, J.P. Gilson, Micropor. Mesopor. Mater. 57 (2003) 297–308.
[16] A.C. Oliveira, A. Tuel, N. Essayem, J.-M. Clacens, Y. Ben Taârit, M.C. Rangel, in: J. Cejka, N. Zilkova, P. Nachtigall (Eds.), Stud. Surf. Sci. Catal., vol. 158, Elsevier, Amsterdam, 2005, p. 1677.
[17] A. Patel, C. Coudurier, N. Essayem, J.C. Védrine, J. Chem. Soc., Faraday Trans. 93 (1997) 247.
[18] L.O. Almanza, Ph.D. Thesis, Université Claude Bernard, France, 1997.
[19] M.L. Poutsma, in: J.A. Rabo (Ed.), Zeolite Chemistry and Catalysis, vol. 171, ACS monograph, ACS Washington, DC, 1976, p. 437.
[20] F.J. Machado, C.M. Lopez, Y. Campos, A. Bolivar, S. Yunes, Appl. Catal. A: Gen. 226 (2002) 241–252.
[21] E. García, M.A. Volpe, M.L. Ferreira, E. Rueda, J. Mol. Catal. A: Chem. 201 (2003) 263–281.
[22] H. Liu, G.D. Lei, W.M.H. Sachtler, Appl. Catal. A: Gen. 137 (1996) 167–177.
[23] J. Kärger, M. Petzold, S. Ernest, J. Weitkamp, J. Catal. 136 (1992) 283.
[24] B.T. Carvill, B.A. Lerner, B.J. Adelman, D.C. Tomczak, W.M.H. Sachtler, J. Catal. 144 (1993) 1–8.
[25] M.M. Mohamed, N.S. Gomaa, M. El-Moselhy, N.A. Eissa, J. Colloid Interf. Sci. 259 (2003) 331–337.
[26] O.E. Lebedeva, W.M.H. Sachtler, J. Catal. 191 (2000) 364–372.
[27] Y. Okamoto, H. Kikiuta, Y. Ohto, S. Nasu, O. Terasaki, Stud. Surf. Sci. Catal. 105 (1997) 2051–2058.
[28] P. Wu, T. Komatsu, T. Yashima, Micropor. Mesopor. Mater. 20 (1998) 139–147.
[29] O. Bortnovsky, Z. Melichar, Z. Sobalík, B. Wichterlová, Micropor. Mesopor. Mater. 42 (2001) 97–102.
[30] V. Adeeva, J.W. Haan, G.D. Lei, V. Schunemann, L.J.M. van de Ven, W.M.H. Sachtler, R.A. van Santen, J. Catal. 151 (1995) 364–372.
[31] H. Liu, V. Adeeva, G.D. Lei, W.M.H. Sachtler, J. Mol. Catal. A: Chem. 100 (1995) 35–48.